ACS APPLIED MATERIALS & INTERFACES

Research Article

www.acsami.org

Prediction of the Percolation Threshold and Electrical conductivity of Self-Assembled Antimony-Doped Tin Oxide Nanoparticles into Ordered Structures in PMMA/ATO Nanocomposites

Youngho Jin and Rosario A. Gerhardt*

School of Materials Science and Engineering, Georgia Institute of Technology, Atlanta, Georgia 30332-0245, United States

Supporting Information

ABSTRACT: Electrical percolation in nanocomposites consisting of poly(methyl methacrylate) (PMMA) and antimony tin oxide (ATO) nanoparticles was investigated experimentally using monosize and polydisperse polymer particles. The nanocomposites were fabricated by compression molding at 170 °C. The matrix PMMA was transformed into space filling polyhedra while the ATO nanoparticles distributed along the sharp edges of the matrix, forming a 3D interconnected network. The measured electrical resistivity showed that percolation was achieved in these materials at a very low ATO content of 0.99 wt % ATO when monosize PMMA was used, whereas 1.48 wt % ATO was needed to achieve percolation when the PMMA was polydispersed. A parametric finite element approach was chosen to model this unique microstructure-driven self-assembling percolation behavior. COMSOL Multiphysics was used to solve the effects of phase segregation between the matrix and the filler using a 2D simplified model in the frequency domain of the AC/DC module. It was found that the percolation threshold (p_c) is affected by the size ratio between the matrix and the filler in a systematic way. Furthermore, simulations indicate that small deviations from perfect interconnection result mostly in changes in the electrical resistivity while the minimum DC resistivity achievable in any given composite is governed by the electrical conductivity of the filler, which must be accurately known in order to obtain an accurate prediction. The model is quite general and is able to predict percolation behavior in a number of other similarly processed segregated network nanocomposites.

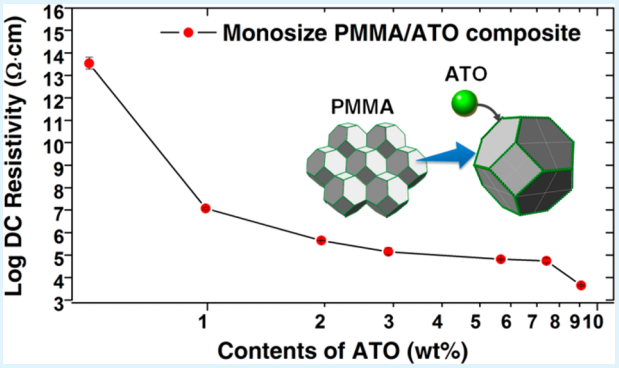

KEYWORDS: *polymer matrix composites (PMCs), nanocomposite, functional composite, electrical properties, finite element analysis (FEA)*

1. INTRODUCTION

Polymer matrix composites have been widely investigated due to their varied applications such as parts in microelectronics, electromagnetic shielding, sensors, antistatic materials, and others.[1−3] Among many polymeric materials, poly(methyl methacrylate) (PMMA) is often used as an insulating matrix in composites, because of its high electrical resistivity. However, accumulation of static charge limits its possible applications, although it possesses good transparency.[1] Different kinds conductive fillers can be used depending on the targeted applications. Carbon based fillers such as carbon black, carbon nanotubes (CNTs), and graphene have been widely used as conductive fillers, resulting in conductivities as high as 10° S/cm for application in sensors, EMI shielding, electronic-nose devices, and novel interconnects.[4−6] Some metallic fillers have also been used to fabricate highly conductive composites.[7,8] Many fabrication methods have been utilized to make the composites, including mechanical blending, solution blending, and latex technology, to make phase segregated conductive polymer composites. Pang and co-workers recently reviewed these processing methods as well as the various matrix and fillers used in different applications.[9] Normally, it is desirable to minimize the amount of filler in polymer matrix composites to lower the cost, to make the processing easier and to maintain balanced properties such as electrical conductivity, transparency, and mechanical strength. Mechanical blending is one of the most effective methods to fabricate a perfect segregated network in the composites.

Transparent oxides such as fluorine-doped tin oxide (FTO),[10] tin-doped indium oxide (ITO),[11] and antimony-doped tin oxide (ATO)[12] have received special attention due to their excellent electro-optical properties.[2] ATO has advantages among them because it is much cheaper than ITO and it shows better performance as an antistatic agent compared to carbon black and other metallic pigments.[13] ATO is usually used as a thin film because it is difficult to form in bulk form due to

Received: September 9, 2014
Accepted: November 27, 2014
Published: November 27, 2014

difficulties in getting a fully dense compact because of nondensification mechanisms of surface diffusion and evaporation.[14,15] In this study, we incorporate ATO as a filler in the PMMA matrix. This composite can find more applications in electronics, optics and sensors due to its distinct combination of electrical and optical properties.

We have reported on several insulator−conductor composite systems previously, which showed unique electrical percolation at low concentration of fillers.[1,15−19] The schematic representation of this percolation is shown in Figure 1.

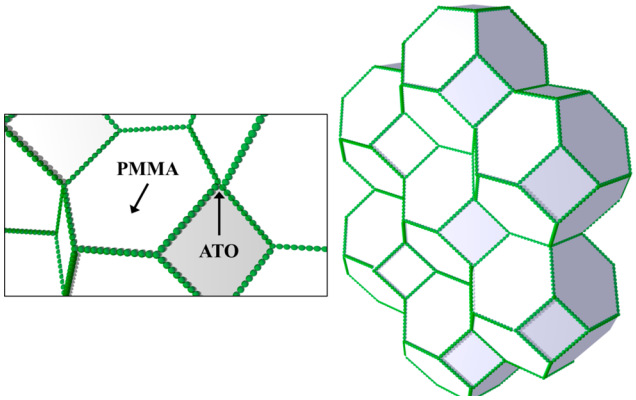

Figure 1. Schematic of segregated distribution of nanoparticles along the edges of matrix microspheres that transformed into truncated octahedra.

The matrix microspheres undergo viscoelastic movement during compression molding. The restacking and reorientation occurs in this stage. Then the deformation at the contact points is followed. At this stage, densification of the matrix spheres or coalescence takes place.[20] However, the coalescence of the polymer is prevented by the presence of nanoparticles on the surface of the matrix spheres.[21] This results in the shape transformation of the matrix into a faceted polyhedra, and the rearrangement of nanoparticles along the edges of the matrix (Figure 1).

The main purpose of this study was to compare the effect of varying the size distribution of the matrix polymer particles on the percolation behavior and electrical resistivity of self-assembled nanocomposites and to model their percolation behavior in detail using finite element analysis and a simplified 2D model.

2. EXPERIMENTAL SECTION

2.1. Raw Materials and Composite Fabrication. The monosize PMMA was obtained from Cospheric LLC. The particle size was in the range of 90−106 μm (Figure 2a). The polydisperse PMMA was obtained from Buehler Ltd. (Transoptic powder). The particle size was in the range of 10−100 μm (Figure 2b) and the average size was 52.4 ± 4.37 μm with a standard deviation of 27.8 μm. The ATO nanoparticles, containing 10 wt % Sb_2O_5 to SnO_2, were obtained from Alfa Aesar (Ward Hill, MA). According to the manufacturer, the size range was 20−40 nm. From the transmission electron microscopy (TEM) micrographs (Figure 2c), the average size was found to be close to this value. The glass transition temperature and the melting temperature of PMMA were 102 and 286 °C, respectively, as obtained by differential scanning calorimetry. The PMMA and ATO nanoparticles were mechanically blended for 10 min in the blender at room temperature as described in our previous papers.[1,17,18,22,23] The surface of the PMMA microspheres was covered with ATO nanoparticles. The nanoparticles on the surface of the matrix were uniformly distributed as blending time increased. However, care must be taken to avoid localized heating in the blender, which can partially liquefy some polymer spheres and decrease the connectivity of the filler-chain network during compression molding. The conductive nanoparticles can be surface modified for better interaction with the polymer matrix. However, doing so might prevent good electrical contact between the nanoparticles. Therefore, ATO particles were not surface modified prior to blending. The composition of PMMA/ATO composites was varied between 0.49 and 9.09 wt %. The ATO coated PMMA microspheres were compression molded using a Struers mounting press at 170 °C for 15 min. The pressure applied during molding was 50.68 MPa. The nanocomposites were hot pressed as disks with diameter of 31.7 mm. The sample thickness was controlled to be 2.0 mm.

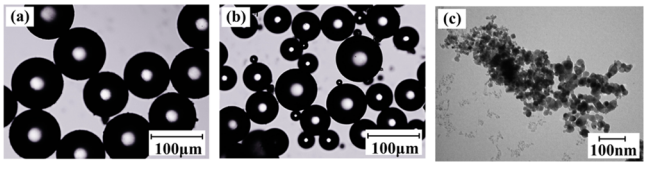

Figure 2. Optical images of (a) monosize PMMA, (b) polydisperse PMMA, and (c) TEM image of ATO nanoparticles.

2.2. Electrical Characterization. A Solartron 1260 impedance analyzer was used together with a Solartron 1296 Dielectric Interface (Solartron Analytical, Farnborough, Hampshire, U.K.), for the electrical characterization of the nanocomposites. All samples were scanned with frequencies ranging from 10 MHz−0.1 Hz using an AC voltage of 500 mV. Prior to impedance measurements, a Denton Vacuum Desk II turbo sputter coater (Denton Vacuum, Moorestown, NJ) was used to coat the samples with Ag (nominal purity of 99.9%) as the contact electrodes. Impedance is a complex quantity that has a real part and an imaginary part, which allows rapid detection of changes in the electrical response with respect to frequency. In other words, it is an excellent method for detecting percolation in insulator−conductor nanocomposites.[24] The DC resistance values were obtained from the intercepts on the real impedance axis of the complex impedance plots (Z″ vs Z′), then converted into resistivity values taking the dimensions of the samples into account. However, it is not uncommon for only a small part of the semicircles to appear in the complex plots in the more insulating or dielectric materials. To obtain the intercepts, the curves were fitted using constant phase element (CPE) in parallel with the equivalent circuit of a resistance. This method is well described elsewhere (see the Supporting Information).[17,25]

2.3. Microstructural Characterization. A Hitachi S3700 (Dallas, TX) SEM instrument was used for microstructural characterization. Selected samples were polished with silicon carbide paper and alumina polishing solution. It is important to postprocess composite samples below the glass transition temperature to avoid polymer flow and deformation.[17,22] The Hitachi S3700 SEM instrument enables charge-free imaging of dielectric samples without gold coating by low vacuum observation at 6−270 Pa (7 mT−2 Torr). All specimens were scanned in variable pressure mode with backscattered detector using 15 kV and 40−50 Pa.

3. RESULTS AND DISCUSSION

3.1. Electrical Conductivity Percolation Curves of PMMA and ATO Nanocomposites. DC resistivity values were obtained from the intercepts of complex impedance curves onto the real impedance axis considering sample geometry as described previously.[17] Figure 3 represents DC resistivity as a function of ATO content. Electrical percolation is apparent at 1.48 wt % (0.27 vol %) for the size distributed PMMA(10−100 μm) and 0.99 wt % (0.18 vol %) for the monosize PMMA as a matrix, where the electrical resistivity

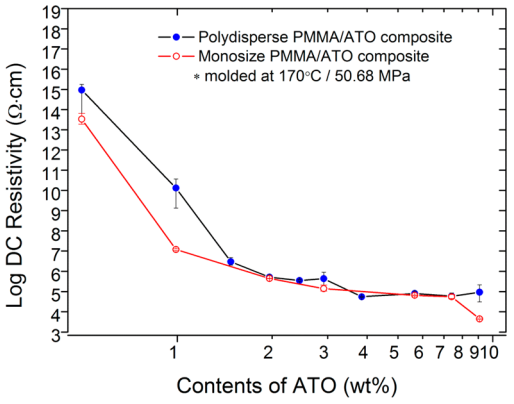

Figure 3. DC resistivity of PMMA/ATO nanocomposites as a function of ATO content (molded at 170 °C, 50.6 MPa for 15 min).

decreases by about 9 orders of magnitude. The percolation threshold is mostly affected by the size ratio of the matrix and the filler ($p_c \propto (1/(r_{matrix}/r_{filler}))$, where the larger the ratio is, the lower p_c is.[26] In this study, it was found that the percolation threshold is lower for the composites made with the monosize starting materials primarily because the size ratio between the matrix and the filler is larger than in the polydisperse samples. These results are consistent with other insulator−conductor composites fabricated by a similar procedure,[1,15−18] all of which percolate at much smaller volume fractions than the theoretically estimated and previously reported values.[27] It is certain that the sharp decrease in DC resistivity is due to the onset of the first chain of conductive particles.

Figure 4 shows the magnitude of the impedance as a function of frequency for the two sets of samples measured. These graphs further illustrate the effect of the starting PMMA size distribution, where the change from the insulating behavior to the conducting behavior occurs at different ATO content values and the critical frequency at which this occurs shifts to a different value.[17] The composites with the ATO concentration below p_c remain frequency dependent throughout the frequency range. Insulating materials normally show this frequency dependent behavior, which is characteristic of a capacitive behavior.[25] In contrast, the composites with the ATO concentration above p_c show a frequency independent behavior (i.e., plateau region) at low frequencies, which is characteristic of conducting materials. This reflects the onset of the first continuous chain of nanoparticles. The plateau region becomes wider as the ATO content increases, until only the conducting behavior is observed, as seen for the 9.09 wt % sample in Figure 4a made with the monosize PMMA. The changes are related to the number of ATO nanoparticle chains that are connected (see Figure 5). Frequency dependent to independent transitions appear at the critical frequency (f_c), which is also marked on the plots in Figure 4. The impedance is exponentially proportional to the frequency above the critical frequency according to the power law, $\sigma(\omega) \propto \omega^x$.[23] It can be seen that for samples with composition near the percolation threshold, f_c moves to a higher frequency for the homogeneous PMMA composites as compared to the polydisperse materials. It is also notable that the composites made with the monosize materials are able to reach a lower resistivity than those made with the polydisperse materials (e.g., see data for 9.09 wt %). More information regarding the critical frequency as a function of composition has been described elsewhere.[22,23]

3.2. Correlation between Microstructures and Electrical Properties. Figure 5a,d displays SEM micrographs obtained using a backscattered detector at the accelerating voltage of 15 kV in variable pressure mode SEM (40 Pa). All images were taken from polished surfaces of the specimens main surface. The images show that the microstructure of these composites consists of ordered arrays of nanoparticles that form nanowire-like interconnections along the particle edges. In the microstructure, the polymer matrix appears dark and the ATO nanoparticles appear as the bright regions, as would be expected because the density of ATO is 5 times greater than that of PMMA. The pressure transmitted to the polymer matrix during compression molding results in shape transformation of the matrix particles into space filling polyhedra, because it is thermodynamically more stable.[28,29] Figure 5a,c shows the polydisperse PMMA composites with compositions of 0.49 and 5.66 wt %, whereas Figure 5b,d shows composites made with the monosize PMMA containing the same amounts of ATO, respectively. It is clear that the monosize materials give a more ordered structure, which, in turn, allow for better properties.

The electrical resistivity curves, shown in Figure 3, decreased by about 7 orders of magnitude, when the first continuous

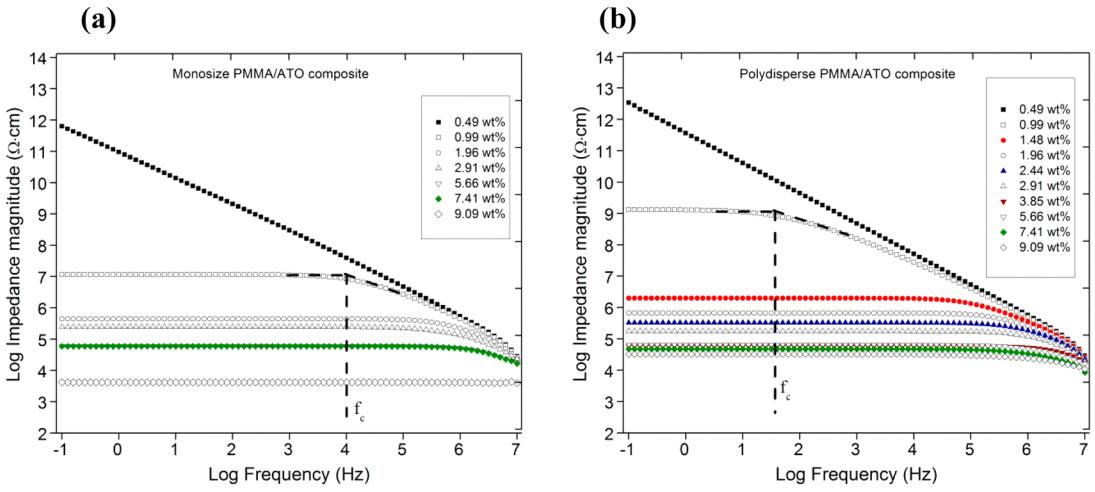

Figure 4. Impedance magnitude of PMMA/ATO nanocomposites for different ATO contents (molded at 170 °C, 50.6 MPa for 15 min) using (a) monosize PMMA and (b) polydisperse PMMA.

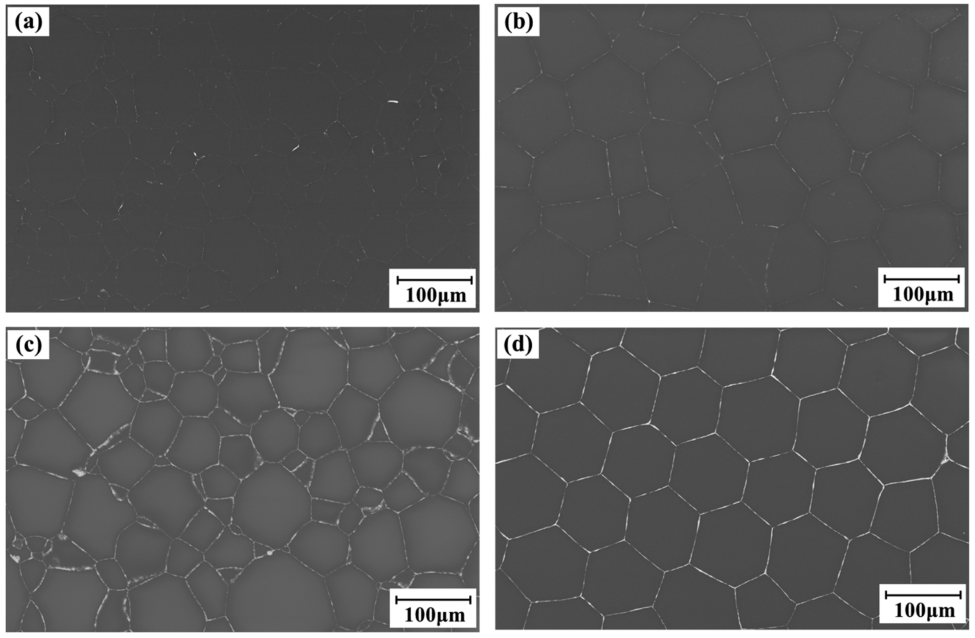

Figure 5. SEM images of polished surfaces of PMMA/ATO nanocomposites containing 0.49 and 5.66 wt % ATO for the polydisperse PMMA (shown in panels a and c) and the monosize PMMA (shown in panels b and d), respectively.

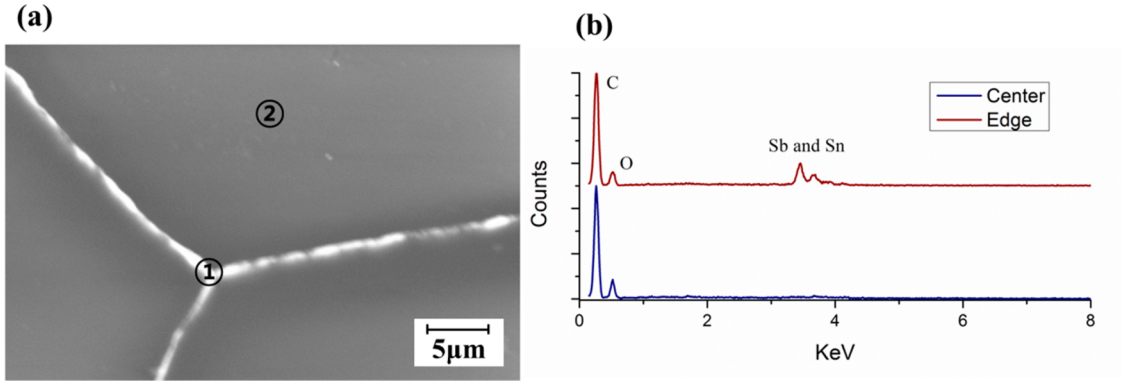

Figure 6. (a) SEM image of nanocomposite (5.66 wt % ATO). (b) EDS spectra at different locations: ① edge; ② center.

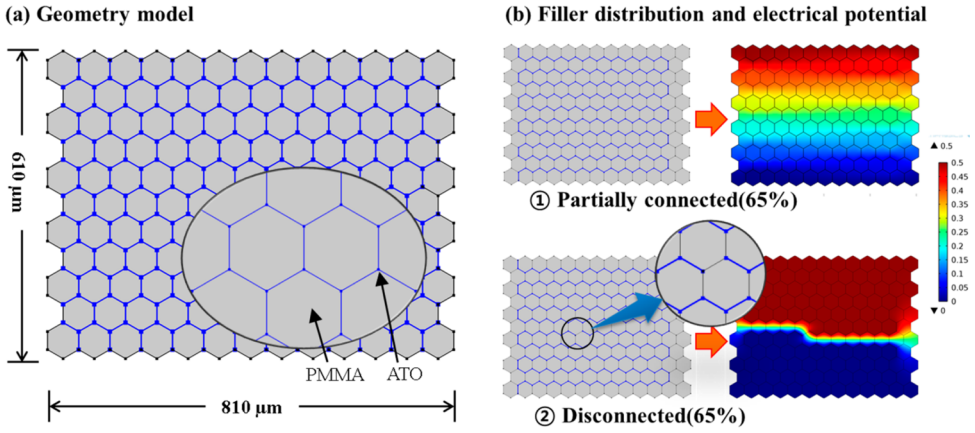

Figure 7. Schematic of the 2D model used for impedance calculations of PMMA-ATO nanocomposites. (a) 2D simplified geometry and (b) filler distribution (partially connected and disconnected) and the corresponding calculated electrical potentials.

chain of conductive nanoparticle was achieved. In the composites with a low filler content of 0.49 wt % (Figure 5a,b), the boundaries are not clearly detected. As the filler content is increased to 5.66 wt %, the boundaries become more detectable (Figure 5c,d). In the composites with the filler contents below the percolation threshold (<1.48 wt %), the nanoparticles are accumulated along the edges without direct physical contact through the volume (see Figure 5a,b).

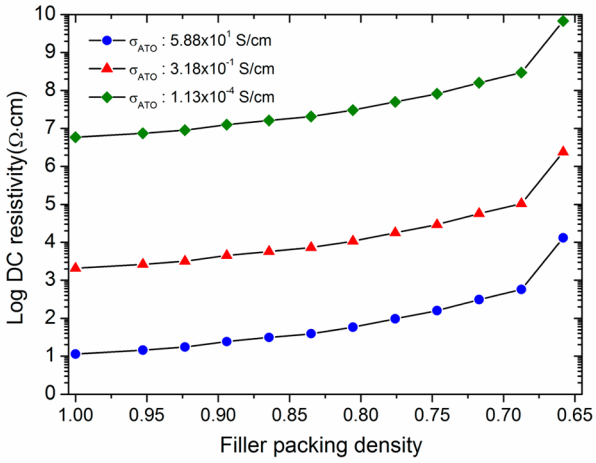

σ_{ATO} (S/cm)	Conditions	Ref.
5.88×10^{1}	Spin coated film	[32]
3.18×10^{-1}	Compressed powder	[33]
1.13×10^{-4}	Hot pressed bulk	[33]

Figure 8. Filler packing density model, "1.0" illustrates perfect solid filler chains and "0.65" illustrates the minimum nanoparticle density needed to maintain the percolated state.

Therefore, the current path through the boundaries of the matrix is not clear in those samples. In contrast, for the composites with the filler contents above the percolation threshold (>1.48 wt %), the SEM images show more noticeable boundaries (Figure 5c,d).

Although the microstructures provide strong evidence of the filler location, energy dispersive spectroscopy (EDS) was used to confirm it. Two different locations (the center and the edge of matrix) in the composite were scanned, as shown in Figure 6a and labeled ① and ②. The EDS spectra (shown in Figure 6b) showed strong peaks of Sb and Sn in the edge scans (region labeled ①), while no Sb or Sn peak was detected in the center of a polymer grain (labeled region ②). It is clear that the viscoelastic motion of PMMA during compression pressing forces the ATO particles to be aligned in the boundaries of the matrix. And the presence of ATO in the boundary prohibits the polymer coalescence, which in turn produces this microstructure. This is consistent with our previous reports on other composites systems.[15,26]

4. FEA MODELING RESULTS AND DISCUSSION

4.1. Use of COMSOL Multiphysics. Electrical percolation is possible in insulator−conductor nanocomposites at very low concentrations of fillers, when using the fabrication conditions reported in our previous papers.[1,15−18,22,23] This concept can be applicable to all kinds of insulator−conductor composites and not just those mentioned here. It is very important to understand the mechanisms of this percolation to expand the possible applications. In this study, we used a finite element approach to solve the electric potential in the AC environments to calculate the impedance and resistivity using a simplified 2D model for the insulator−conductor composites (see Figure 7).

The modeling steps used in this study include:

1. Selecting the mode in the COMSOL Multiphysics AC/DC module.
2. Drawing the composite geometries.
3. Generating the mesh.
4. Defining the electrical properties in the domains and boundary conditions.
5. Solving and finding the field distributions.
6. Using the postprocessing capabilities in COMSOL Multiphysics to compute impedance and related electrical quantities.

The numerical simulations were performed in the frequency domain using the AC/DC module of COMSOL Multiphysics Version 4.4. The objective was to solve the quasi-static form of Maxwell's equations for the electric potential in the 2D simplified case. The percolation model possessing a segregated filler distribution, with Voronoi-type matrix arrangement[23,30] was adopted to describe the simplified 2D geometry. The nanoparticles can be described as separate domains or as boundary conditions. Solutions to both cases provided the same values of the electrical quantities. Various filler distributions in the 2D geometry were investigated to describe the interconnectivity of nanoparticles along the edges of the matrix particles. Figure 7 shows a schematic of the geometric model as well as two possible filler distributions, i.e., a partially connected filler distribution and a disconnected filler distribution. On the right of the image, one can see the changes in the electrical potential for the two different filler distributions.

4.2. Impedance Simulation of PMMA/ATO Nanocomposites. The impedance of the nanocomposites was obtained by postprocessing of the solved electric potential as described previously.[31] The impedance simulation using perfect filler networks can predict the percolation threshold of phase segregated composites if the size ratio between the matrix and the filler is known. It can also predict the minimum electrical resistivity of the composite assuming that there is no size distribution in the matrix and the filler, and the fillers are aligned in a perfect network. However, it needs to be modified to describe real composite systems with size distributions and imperfect filler chains.

To account for these variations, a filler packing density model was introduced to accommodate disconnected filler chains while maintaining the percolated state. Filler packing density is presented as ranging from 1 (perfect network interconnection) to 0.65 (minimum value needed to maintain overall connectivity). Figure 8 shows simulated DC resistivities for different filler chain densities. It can be seen that there is a 3 orders of magnitude difference in DC resistivity from the fully networked state to the barely interconnected state. The DC resistivity at the 65% filler packing density can be considered as

Table 1. Comparison between Experimental Measurements and FEA Simulation Results

		experiments			FEA simulation [σ_{filler}: 0.32(S/cm)]		
composites	r_{filler}/r_{matrix}	p_c (vol %)	$\rho_{percolation}$ (Ω·cm)	ρ_{min} (Ω·cm)	p_c (vol %)	$\rho_{percolation}$ (Ω·cm)	ρ_{min} (Ω·cm)
polydisperse PMMA/ATO	20 nm/25 μm	0.27	1.98×10^6	3.20×10^4	0.21	2.42×10^6	2.08×10^3
monosize PMMA/ATO	20 nm/50 μm	0.18	2.28×10^6	4.11×10^3	0.10		

the resistivity at the percolation threshold, whereas the DC resistivity at the 100% filler packing density can illustrate the theoretical minimum resistivity that may be obtained in phase segregated composites.

Second, the electrical conductivity value of the filler should be representative of the real filler in the composite. Figure 8 also shows the differences in the simulated DC resistivity curves when using different ATO conductivity values. The maximum DC conductivity of ATO can be above 50 S/cm, as determined for spin coated films.[32] However, compressed ATO powder showed 0.318 S/cm, whereas hot pressed ATO showed much lower value due to nondensification mechanism of ATO.[33] It should be noted that the electrical conductivity of compressed ATO powder is the most realistic value to use for the fillers of the phase segregated PMMA composites, considering the possible packing states of ATO nanoparticles that may occur in the composite.[33]

Table 1 shows the comparison between experimental and simulated DC resistivity values. As has been discussed, monosized PMMA/ATO composites showed lower percolation threshold and lower minimum DC resistivity values than polydisperse PMMA/ATO composites, because the monosize matrix a has larger mean particle size and provides better conditions for ideal phase segregation to occur. It can be seen that there is good agreement in the percolation threshold between experimental and simulated results. The FEA model can also predict the DC resistivity at the percolation threshold and saturated state more accurately, with the aid of the filler packing density model and the use of the proper filler electrical conductivity as mentioned earlier. It has to be noted that the minimum DC resistivity achievable in the composite is governed by the electrical conductivity of the filler, when it forms perfect interconnected networks. This was demonstrated with the monosized PMMA composites that formed a nearly perfect filler network, as shown in Figure 5d.

Figure 9 presents simulated impedance curves as a function of frequency for pure PMMA and varying degrees of filler interconnectivity. Electrical percolation was clearly shown when the first continuous chain of filler was connected between the top and bottom electrodes (port and terminal), similarly to what has been examined in the real materials. The onset of the first fully interconnected filler chain was described as the "partially connected (65%)" in the 2D model. The impedance was seen to decrease as additional percolation chains were connected. The transition from the frequency dependent to the frequency independent impedance can be estimated when the filler chain is weakly connected, and was obtained by reducing the conductivity of the chain.

Because there was good agreement between the experimental and modeling results for the PMMA/ATO system, it is promising that this simplified model may be able to estimate the percolation threshold and impedance in various kinds of insulator−conductor segregated network systems, provided that the materials characteristics such as matrix and filler size and electrical conductivity of the filler are known

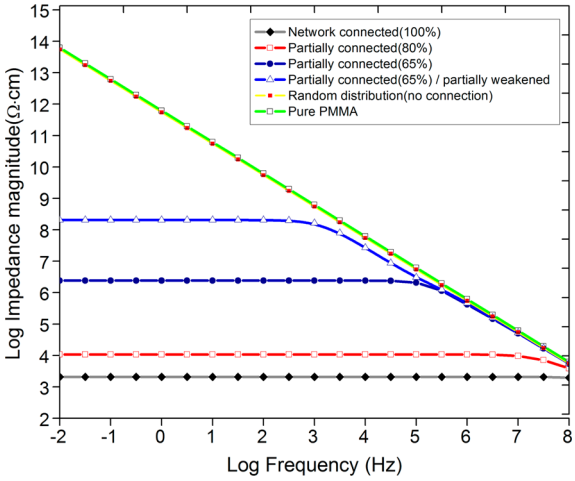

Figure 9. FEA simulated impedance of PMMA/ATO nanocomposites using different path lengths and different degrees of interconnected nanoparticles.

Although the percolation threshold as a function of particle size of the matrix and filler was able to be roughly estimated in our previous studies,[23,26] it needed to be modified to estimate the percolation threshold more accurately. In the current model, the matrix is assumed to be truncated octahedral, as shown in Figure 1. The equivalent volume of the Voronoi types of matrix in terms of initial spherical PMMA particles can be estimated as

$$\frac{4}{3}\pi {r_p}^3 = 11.31 {a_p}^3 \quad (1)$$

where, r_p is the average radius of the PMMA microspheres and a_p is the edge length of the truncated octahedra. Because the filler particles were assumed as cubes, the equivalent volume of filler particle is

$$\frac{4}{3}\pi {r_f}^3 = {a_f}^3 \quad (2)$$

where r_f is the average radius of filler nanoparticles and a_f is the edge length of the filler cube. In the 2D model, the percolation threshold can be estimated as area fraction of the network path connected state, which is given by

$$3a_p \cdot a_f / 1.5\sqrt{3}\, {a_p}^2 \quad (3)$$

Combining eqs 1−3, the area fraction for 2D percolation is given by 2.588 r_f/r_p. This value is slightly smaller than the percolation threshold in the previous geometric model[23,26] because the FEA model assumes perfect distribution of fillers in a single wire rather than using the probability that the filler particles will touch in a given configuration. In addition, the total surface area of the matrix in 3D, an extension of the 2D model, is slightly smaller than that of the real matrix.

Figure 10 displays the change of area fraction in the 2D model, which is equivalent to the volume fraction in the 3D model, as the size ratio between the matrix and the filler

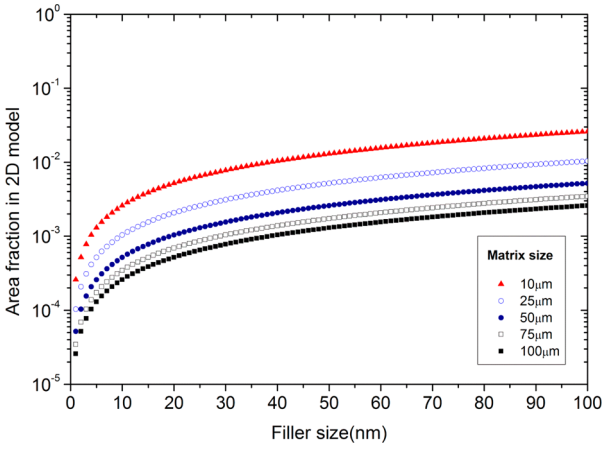

Figure 10. Area fraction as a function of matrix and filler size derived from FEA simulations of 2D idealized segregated network microstructures with truncated octahedral shapes.

changes. It increases as the ratio increases, in other words, the percolation threshold increases as the size of the filler increases and the size of the matrix decreases. These predicted values show good agreement with the experimental results reported above, especially in the case of the nanocomposites that were fabricated with the monosize 100 μm PMMA particles, where p_c was found to be at 0.18 vol % or 0.0018 for a filler size of 40 nm.

5. CONCLUSIONS

The phase segregated PMMA and ATO nanocomposites were made using the same ATO nanoparticles and monodisperse or polydisperse PMMA matrix polymer. Electrical percolation was achieved at very low concentrations of ATO filler (0.99 wt % for the monosize materials and 1.48 wt % for the polydisperse materials).

The finite element approach was selected for determining the impedance of these insulator−conductor nanocomposites, which have phase segregated microstructures. The 2D simplified model was able to predict the percolation threshold and the electrical conductivity of the composites. Good agreement was obtained between the experimental results and the modeling results by using a filler packing density model and a realistic filler conductivity value. The modeling results considered different electrical resistivity responses as well as different states of filler distribution and thus the simulation results are applicable to many different kinds of insulator−conductor composite systems and not just those that were presented here. It was also found that the minimum DC resistivity of the composite is governed by the electrical conductivity of the filler while the percolation threshold is governed by the size ratio between the matrix and the filler. Future simulation studies may include the effects of the surface energy of the fillers and the filler/matrix interactions on the electrical properties of phase segregated conductive composites.

■ ASSOCIATED CONTENT

Supporting Information

Brief description of impedance measurements and analysis and figures showing the complex impedance plots for the 0.49 wt% ATO/PMMA composite fitted using a parallel R-CPE model and for several PMMA/ATO composites. This material is available free of charge via the Internet at http://pubs.acs.org.

■ AUTHOR INFORMATION

Corresponding Author

*R. A. Gerhardt. E-mail: rosario.gerhardt@mse.gatech.edu.

Notes

The authors declare no competing financial interest.

■ ACKNOWLEDGMENTS

Research funding from the National Science Foundation(NSF) under DMR-1207323 is acknowledged and appreciated. TEM image of ATO nanoparticles was obtained by Mr. Jaehan Jung.

■ REFERENCES

(1) Capozzi, C. J.; Gerhardt, R. A. Novel Percolation Mechanism in PMMA Matrix Composites Containing Segregated ITO Nanowire Networks. *Adv. Funct. Mater.* **2007**, *17*, 2515−2521.

(2) Stroppa, D. G.; Montoro, L. A.; Beltrán, A.; Conti, T. G.; da Silva, R. O.; Andrés, J.; Longo, E.; Leite, E. R.; Ramirez, A. J. Unveiling the Chemical and Morphological Features of Sb−SnO_2 Nanocrystals by the Combined Use of High-Resolution Transmission Electron Microscopy and ab Initio Surface Energy Calculations. *J. Am. Chem. Soc.* **2009**, *131*, 14544−14548.

(3) Lu, G.; Li, X.; Jiang, H.; Mao, X. Electrical Conductivity of Carbon Fibers/ABS Resin Composites Mixed with Carbon Blacks. *J. Appl. Polym. Sci.* **1996**, *62*, 2193−2199.

(4) Bao, Y.; Xu, L.; Pang, H.; Yan, D.-X.; Chen, C.; Zhang, W.-Q.; Tang, J.-H.; Li, Z.-M. Preparation and Properties of Carbon Black/Polymer Composites with Segregated and Double-Percolated Network Structures. *J. Mater. Sci.* **2013**, *48*, 4892−4898.

(5) Pham, V. H.; Dang, T. T.; Hur, S. H.; Kim, E. J.; Chung, J. S. Highly Conductive Poly(methyl methacrylate) (PMMA)-Reduced Graphene Oxide Composite Prepared by Self-Assembly of PMMA Latex and Graphene Oxide through Electrostatic Interaction. *ACS Appl. Mater. Interfaces.* **2012**, *4*, 2630−2636.

(6) Liu, Q.; Tu, J.; Wang, X.; Yu, W.; Zheng, W.; Zhao, Z. Electrical Conductivity of Carbon Nanotube/Poly(vinylidene fluoride) Composites Prepared by High-Speed Mechanical Mixing. *Carbon* **2012**, *50*, 339−341.

(7) Gelves, G. A.; Al-Saleh, M. H.; Sundararaj, U. Highly Electrically Conductive and High Performance EMI Shielding Nanowire/Polymer Nanocomposites by Miscible Mixing and Precipitation. *J. Mater. Chem.* **2011**, *21*, 829−836.

(8) Mamunya, Y. P.; Davydenko, V. V.; Pissis, P.; Lebedev, E. V. Electrical and Thermal Conductivity of Polymers Filled with Metal Powders. *Eur. Polym. J.* **2002**, *38*, 1887−1897.

(9) Pang, H.; Xu, L.; Yan, D.-X.; Li, Z.-M. Conductive Polymer Composites with Segregated Structures. *Prog. Polym. Sci.* **2014**, *39*, 1908−1933.

(10) Rakhshani, A. E.; Makdisi, Y.; Ramazaniyan, H. A. Electronic and Optical Properties of Fluorine-Doped Tin Oxide Films. *J. Appl. Phys.* **1998**, *83*, 1049−1057.

(11) Granqvist, C. G.; Hultåker, A. Transparent and Conducting ITO Films: New Developments and Applications. *Thin Solid Films* **2002**, *411*, 1−5.

(12) Terrier, C.; Chatelon, J. P.; Roger, J. A. Electrical and Optical Properties of Sb:SnO_2 Thin Films Obtained by the Sol-Gel Method. *Thin Solid Films* **1997**, *295*, 95−100.

(13) Kim, K. H.; Lee, S. W.; Shin, D. W.; Park, C. G. Effect of Antimony Addition on Electrical and Optical Properties of Tin Oxide Film. *J. Am. Ceram. Soc.* **1994**, *77*, 915−921.

(14) Zhang, J.; Gao, L.; Chen, M. Spark Plasma Sintering of High-Density Antimony-Doped Tin Oxide Ceramics from Nanoparticles. *J. Am. Ceram. Soc.* **2006**, *89*, 3874−3876.

(15) Pruyn, T. L.; Gerhardt, R. A. Percolation in Borosilicate Glass Matrix Composites Containing Antimony-Doped Tin Oxide Segregated Networks. Part I: Fabrication of Segregated Networks. *J. Am. Ceram. Soc.* **2013**, *96*, 3544−3551.

(16) Mason, C.; Gerhardt, R. Fabrication of Transparent, Conductive Phase-Segregated ITO/PC Composites. *MRS Online Proc. Libr.* **2010**, *1257*, DOI:10.1557/PROC-1257-O03-50.
(17) Ou, R.; Gupta, S.; Parker, C. A.; Gerhardt, R. A. Fabrication and Electrical Eonductivity of Poly(methyl methacrylate) (PMMA)/Carbon Black (CB) Composites: Comparison between an Ordered Carbon Black Nanowire-like Segregated Structure and a Randomly Dispersed Carbon Black Nanostructure. *J. Phys. Chem. B* **2006**, *110*, 22365−22373.
(18) Gupta, S.; Ou, R.; Gerhardt, R. Effect of the Fabrication Method on the Electrical Properties of Poly(acrylonitrile-co-butadiene-co-styrene)/Carbon Black Composites. *J. Electron. Mater.* **2006**, *35*, 224−229.
(19) Bertram, B. D.; Gerhardt, R. A.; Schultz, J. W. Impedance Response and Modeling of Composites Containing Aligned Semiconductor Whiskers: Effects of dc-Bias Partitioning and Percolated-Cluster Length, Topology, and Filler Interfaces. *J. Appl. Phys.* **2012**, *111*, DOI: 10.1063/1.4729119.
(20) Jog, J. P. Solid State Processing of Polymers: A Review. *Adv. Polym. Technol.* **1993**, *12*, 281−289.
(21) Greco, A.; Maffezzoli, A. Polymer Melting and Polymer Powder Sintering by Thermal Analysis. *J. Therm. Anal. Calorim.* **2003**, *72*, 1167−1174.
(22) Capozzi, C. J.; Gerhardt, R. A. Correlation of the ac Electrical Conductivity and the Microstructure of PMMA/ITO Nanocomposites That Possess Phase-Segregated Microstructures. *J. Phys. Chem. C* **2008**, *112*, 19372−19382.
(23) Capozzi, C. J.; Li, Z.; Samuels, R. J.; Gerhardt, R. A. Impedance Spectroscopy and Optical Characterization of Polymethyl Methacrylate/Indium Tin Oxide Nanocomposites with Three-Dimensional Voronoi Microstructures. *J. Appl. Phys.* **2008**, *104*, 114902.
(24) Gerhardt, R. A.; Runyan, J.; Sana, C.; McLachlan, D. S.; Ruh, R. Electrical Properties of Boron Nitride Matrix Composites: III, Observations near the Percolation Threshold in BN−B_4C Composites. *J. Am. Ceram. Soc.* **2001**, *84*, 2335−2342.
(25) Gerhardt, R. A. Impedance Spectroscopy and Mobility Spectra. In *Encyclopedia of Condensed Matter Physics*; Bassani, F., Liedl, G. L., Wyder, P., Eds.; Elsevier: Oxford, U. K., 2005; pp 350−363.
(26) Waddell, J.; Ou, R.; Capozzi, C. J.; Gupta, S.; Parker, C. A.; Gerhardt, R. A.; Seal, K.; Kalinin, S. V.; Baddorf, A. P. Detection of Percolating Paths in Polyhedral Segregated Network Composites using Electrostatic Force Microscopy and Conductive Atomic Force Microscopy. *Appl. Phys. Lett.* **2009**, *95*, 233122.
(27) Lux, F. Models Proposed to Explain the Electrical Conductivity of Mixtures Made of Conductive and Insulating Materials. *J. Mater. Sci.* **1993**, *28*, 285−301.
(28) Narkis, M. Size Distribution of Suspension-Polymerized Unsaturated Polyester Beads. *J. Appl. Polym. Sci.* **1979**, *23*, 2043−2048.
(29) Kuczynski, G. C.; Neuville, B.; Toner, H. P. Study of Sintering of Poly(methyl methacrylate). *J. Appl. Polym. Sci.* **1970**, *14*, 2069−2077.
(30) Bhattacharyya, S. K.; Basu, S.; De, S. K. Effect of Size, Shape and Oxide Content of Metal Particles on the Formation of Segregated Networks in PVC Composites. *Composites* **1978**, *9*, 177−183.
(31) Kumar, S.; Gerhardt, R. A. Role of Geometric Parameters in Electrical Measurements of Insulating Thin Films Deposited on a Conductive Substrate. *Meas. Sci. Technol.* **2012**, *23*, 035602.
(32) Goebbert, C.; Nonninger, R.; Aegerter, M. A.; Schmidt, H. Wet Chemical Deposition of ATO and ITO Coatings Using Crystalline Nanoparticles Redispersable in Solutions. *Thin Solid Films* **1999**, *351*, 79−84.
(33) Pruyn, T. L.; Gerhardt, R. A. Detection of Different Interfaces in Percolated Networks of Antimony Tin Oxide: Borosilicate Glass Composites by Impedance Spectroscopy. *J. Am. Ceram. Soc.* **2014**, DOI: 10.1111/jace.13269.